Advances in Science and Technology Research Journal

*Advances in Science and Technology Research Journal*, 2025, 19(9), 189–202
https://doi.org/10.12913/22998624/207336
ISSN 2299-8624, License CC-BY 4.0

Received: 2025.05.12
Accepted: 2025.07.15
Published: 2025.08.01

# A novel crow search algorithm-based maximum power point tracking method for wind energy conversion systems

Mouna Ben Smida[1*], Anis Sakly[1]

[1] Laboratory of Automatic, Electrical Systems and Environment, the National Engineering School of Monastir, University of Monastir, Tunisia
* Corresponding author's e-mail: mouna.bensmida@esprim.tn

## ABSTRACT

This study presents an intelligent maximum power point tracking (MPPT) control strategy for variable-speed wind turbine generators, based on the crow search algorithm (CSA) to maximize power generation under wind fluctuations. The proposed CSA-based MPPT method is designed to improve the dynamic response and efficiency of wind energy conversion systems by effectively tracking the optimal operating point. The performance of the CSA-based approach is compared with a conventional torque regulation method, evaluating key metrics such as convergence speed and robustness under turbulent wind conditions. Simulation results demonstrate that the CSA-based MPPT controller outperforms the conventional method, achieving faster convergence to the maximum power point, reduced power oscillations, and improved energy capture efficiency. The results highlight the potential of bio-inspired algorithms like CSA in advancing MPPT control for renewable energy systems, offering a promising alternative to traditional methods for enhancing the performance and reliability of wind turbine generators.

**Keywords:** wind turbine; maximum power point tracking; crow search algorithm; torque regulation; grid.

## INTRODUCTION

A global shift to renewable energy becomes critical to ensure the energy security and address the increasing challenges of climate change and environmental degradation. Among renewable energy technologies, wind energy has emerged as one of the most promising and rapidly growing sectors, contributing significantly to the global energy mix. the global wind energy council states that the total installed capacity of wind power capacity reached 743 GW by the end of 2022, representing an annual growth rate of 12.4% [1].

Wind turbines play a crucial role in harnessing this abundant and clean energy source [2]. However, the efficiency of wind energy conversion systems (WECS) heavily depends on the ability to extract maximum power from the turbine under varying wind conditions. In this context, maximum power point tracking (MPPT) algorithms are an appropriate problem-solving method for complicated issues in the area of renewable energy systems.

Many attempts have been made in recent years to optimize WECS production and the optimization of MPPT in wind turbines has been extensively studied, with various techniques developed to address the challenges posed by dynamic wind conditions [2]. In this context, several researchers in [3,4] investigated traditional methods, i.e., incremental conductance (INC) and perturb and observe (P&O). While these techniques are generally adopted for their simplicity, they suffer from instabilities around the maximum power point and exhibit slow convergence, particularly under highly variable wind conditions. Hannachi et al. in [5], have developed a comparative study of four conventional MPPT techniques and demonstrated the efficiency and the superiority of the Optimal Torque (OT) technique compared to the other MPPTs studied. Advanced techniques through recent works [6, 7] including fuzzy logic control (FLC) and artificial network (ANN)-based

MPPT, offer improved robustness and adaptability. FLC utilizes linguistic rules to dynamically adjust the operating point, while NN-based methods leverage machine learning to model the nonlinear relationship between wind speed, rotor speed, and power output [8,9]. However, these methods typically demand an extensive training data and a high computational resource.

In this framework metaheuristic algorithms, including genetic algorithm (GA), particle swarm optimization (PSO) and crow search algorithm (CSA), have emerged as promising alternatives due to their ability to handle complex, multimodal optimization problems [10].

PSO, inspired by the social behavior of birds, excels in global search capabilities as studied by Bouchakour et al. [11], while GA mimics natural selection to evolve optimal solutions over generations [12]. Ben Smida et al. [13] exploited CSA technique in MPPT studies. This method is based on a novel algorithm inspired by crow foraging behavior. It has demonstrated fast convergence and effective balancing of exploration and exploitation, making it particularly suitable for MPPT in renewable systems. Several studies have suggested improvements in these smart techniques and investigated hybrid approaches, such as hybrid firefly PSO and GA-ANN [14–16]. These techniques combine the strengths of multiple algorithms to enhance performance, particularly under partial shading in photovoltaic systems and turbulent wind conditions in wind turbines — the latter being the focus of the present study.

Despite these advancements, challenges remain in achieving real-time implementation and reducing computational complexity, highlighting the requirement for further research in this area [17]. Compared to other bio-inspired MPPT techniques such as PSO, ant colony optimization (ACO), and GA, the CSA offers a unique balance between exploration and exploitation, combined with a simple implementation structure. This study builds upon these advantages by tailoring CSA specifically for dynamic wind energy environments.

This paper proposes the use of CSA, a novel metaheuristic optimization technique inspired by the intelligent foraging behavior of crows, to enhance MPPT control in wind turbines. CSA is characterized by its simplicity, fast convergence, and adaptive search capabilities, making it particularly suitable for dynamic optimization problems like MPPT. By integrating CSA into the MPPT control strategy, this study aims to improve the efficiency, accuracy, and reliability of power extraction from wind turbines under variable wind conditions. Compared to the conventional torque control technique, the proposed method seeks to provide improved power smoothing and to minimize output power fluctuations.

The primary objectives of this research are:

- to develop a CSA-based MPPT control strategy for wind turbines,
- to evaluate the performance of the proposed method compared to traditional MPPT techniques,
- to validate the performance of the technique in handling dynamic and unpredictable wind conditions.

The remainder of the presented work is organized as outlined below: A detailed representation of the WECS operating in grid-connected mode is developed in Section 2. The machine-side control architecture is explored in Section 3, while Section 4 examines the grid-side control. Section 5 details the development of the proposed MPPT control techniques, and Section 6 discusses the simulation results and performance analysis. Finally, a summary of the main conclusions and potential directions for future research are presented in Section 7, which concludes the paper.

The originality of this work lies in the integration of the CSA with adaptive torque regulation for MPPT under varying wind conditions. Unlike classical methods relying on PI regulators or fuzzy logic controllers, the proposed approach combines global search capabilities with real-time responsiveness, providing improved tracking accuracy and power stability.

## MODELING OF THE GRID CONNECTED WIND TURBINE SYSTEM

The studied WECS includes a direct-drive permanent magnet synchronous generator (PMSG) as shown in Figure 1. It is interfaced with the electrical grid via a back-to-back power conversion stage. This interface consists of two converters operating in coordination to manage the energy flow and system dynamics: a machine side converter (MSC) that is designed to achieve MPPT, and a grid side converter (GSC) designed to stabilize the DC link voltage at the rated value and to control the reactive power.

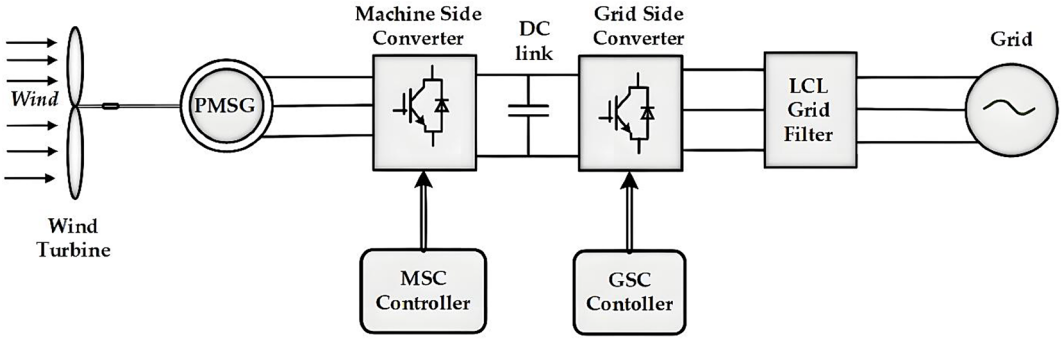


**Figure 1.** Configuration of the grid connected WECS

## Modeling of wind turbine system

The output power of the wind turbine is introduced by [18]:

$$P_w = \frac{1}{2}\rho \Pi R^2 V_w^3 C_p(\lambda, \beta) \quad (1)$$

The power coefficient $Cp$ depends on the tip speed ratio (TSR) $\lambda$ and the blade pitch angle $\beta$. According to Smida and Sakly [19], it can be formulated as follows:

$$C_p(\lambda, \beta) =$$

$$= 0.53 \left[\frac{151}{\lambda_i} - 0.58\,\beta - 0.002\,\beta^{2.14} - 13.2\right] \exp\left(\frac{-18.4}{\lambda_i}\right) \quad (2)$$

where:

$$\lambda_i = \frac{1}{\frac{1}{\lambda - 0.02\beta} - \frac{0.003}{\beta^3 + 1}} \quad (3)$$

$\lambda$ is expressed in equation (4):

$$\lambda = \frac{R\omega}{V_w} \quad (4)$$

The relationship between $Cp$ and λ is depicted in Figure 2. Based on Equation 5, the turbine torque is expressed as:

$$T_m = \frac{P_w}{\omega} \quad (5)$$

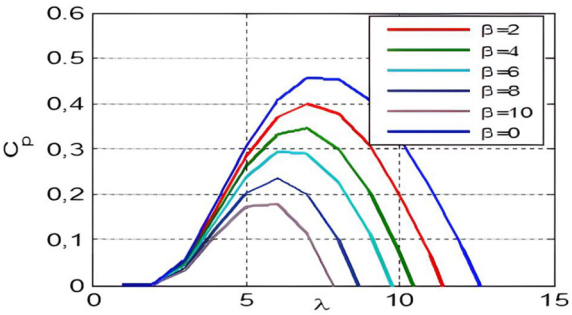


**Figure 2.** Power coefficient curve for different pitch angle values

The expression for the turbine's mechanical speed is derived from the fundamental dynamic relation as follows:

$$J\frac{d\Omega}{dt} = T_m - T_{em} - f\omega \quad (6)$$

The operation and control strategies of a WECS as wind speed increases are typically categorized into four distinct regions as given in Figure 3. Region I is characterized as a spin-up phase during which energy conversion does not

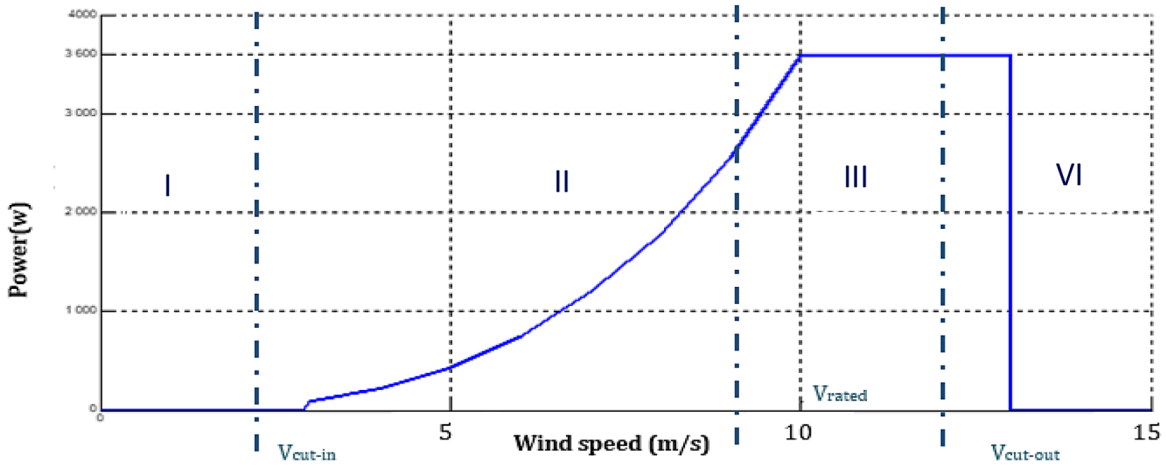


**Figure 3.** Basic operating characteristic of a wind turbine

occur due to insufficient wind speed. Once the wind speed $V_w$ surpasses the cut-in speed ($V_{cut\text{-}in}$) typically ranging from 4 to 3 m/s for small wind turbines (WTs), energy conversion begins. During this phase, the generator torque is used to control the WT speed, ensuring maximum power extraction at each wind speed based on the turbine's characteristics. Region II, the partial-load region, extends up to the wind speed at which the generator reaches its nominal angular speed ($\omega_{gn}$). Typically, this wind speed is lower than the WT's nominal wind speed ($V_{rated}$).

In Region III, the full-load region, during high-wind operation, the WT is controlled to limit the power output to $P_n$ at a maximum allowable angular speed. This is achieved either by increasing the pitch angle in variable-pitch WTs. If the wind speed exceeds a specified cut-out speed ($V_{cut\text{-}out}$) the WECS is shut down to prevent structural damage [20]. This study primarily concentrates on the development of the MPPT control in the second region.

## Generator side modeling

The synchronous generator operates with a shaft speed that is synchronized with the rotating magnetic field. The PMSG is modeled using the Park reference frame where:

$$\frac{d\theta}{dt} = \omega_r \tag{7}$$

The equations developing the ($d$, $q$) generator model expressed are as follows [21]:

$$\begin{cases} v_{sd} = R_s i_{s_d} + \frac{d\varphi_{sd}}{dt} - \omega_r \varphi_{sq} \\ v_{sq} = R_s i_{sq} + \frac{d\varphi_{sq}}{dt} + \omega_r \varphi_{sd} \\ T_{em} = \frac{3}{2} p \varphi i_{sq} \end{cases} \tag{8}$$

$$\begin{cases} \varphi_{sd} = L_s i_{sd} + \varphi \\ \varphi_{sq} = L_s i_{sq} \end{cases} \tag{9}$$

Using the established equations, the system representation is expressed by:

$$\begin{cases} \dot{X} = [A].X + [B].U \\ Y = [C].X + [D].U \end{cases} \tag{10}$$

In matrix form, the model is:

$$\frac{d[X]}{dt} = [A].X + [B].U \tag{11}$$

With:

$$[X] = \left[i_{sd}\ i_{sq}\right]^T \tag{12}$$

$$[U] = \left[v_{sd}\ v_{sq}\ \varphi\right]^T \tag{13}$$

$$\begin{bmatrix} \frac{di_{sd}}{dt} \\ \frac{di_{sq}}{dt} \end{bmatrix} = \begin{bmatrix} -\frac{R_s}{L_s} & \omega_r \\ -\omega_r & -\frac{R_s}{L_s} \end{bmatrix} \cdot \begin{bmatrix} i_{sd} \\ i_{sq} \end{bmatrix} + \begin{bmatrix} \frac{1}{L} & 0 & 0 \\ 0 & \frac{1}{L} & \frac{-\omega_r}{L} \end{bmatrix} \cdot \begin{bmatrix} v_{sd} \\ v_{sq} \\ \varphi \end{bmatrix} \tag{14}$$

## Modeling of the power converters

Two cascaded voltage converters connected via a DC bus ensure power conversion. The detailed model of this electronic interface has been the subject of several studies. The same modelling approach for the three-phase converter applies to both the rectifier and the inverter. This converter is represented in Figure 4. It consists of three IGBT arms, each comprising two switching cells connected in series, operating alternately. In an ideal case, each cell can be approximated as either an open or closed switch. The complementary control signals for the switches are defined by the PWM technique used. Each switch is associated with a switching function equal to 1 in the closed state and 0 in the open state.

The two switching variable conditions for each arm are given by:

$$\gamma_k = \begin{cases} 1, (S_{1k} = 1 \text{ and } S_{2k} = 0) \\ 0, (S_{1k} = 0 \text{ and } S_{2k} = 1) \end{cases} k \in \{1,..,6\} \tag{15}$$

The modulated line-to-line voltages are derived from the DC bus voltage and the switching functions according to:

$$\begin{cases} U_{m_{13}} = (S_{11} - S_{13}).V_{dc} \\ U_{m_{13}} = (S_{12} - S_{23}).V_{dc} \end{cases} \tag{16}$$

The modulated phase voltages are given by the following expressions:

$$\begin{cases} V_{ma} = \frac{2}{3} U_{m13} - \frac{1}{3} U_{m23} \\ V_{mb} = \frac{2}{3} U_{m23} - \frac{1}{3} U_{m13} \end{cases} \tag{17}$$

By combining the equations, we obtain the following matrix form:

$$\begin{pmatrix} V_{ia} \\ V_{ib} \\ V_{ic} \end{pmatrix} = \frac{U_{dc}}{3} \begin{bmatrix} 2 & -1 & -1 \\ -1 & 2 & -1 \\ -1 & -1 & 2 \end{bmatrix} \begin{pmatrix} S_{11} \\ S_{12} \\ S_{13} \end{pmatrix} \tag{18}$$

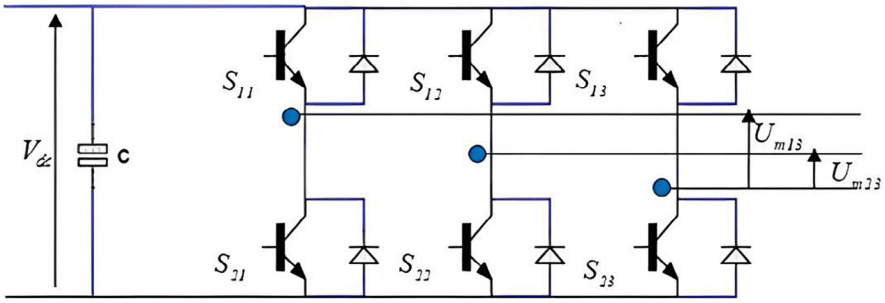


**Figure 4.** Equivalent diagram of the power converter

### Gride side modeling

The dynamic model of the grid, incorporating an inductance filter $L_f$ to mitigate harmonics, can be expressed as follows:

$$\begin{cases} V_{g_d} = V_{i_d} + L_f \frac{di_{g_d}}{dt} + \omega_g L_f i_{g_q} \\ V_{g_q} = V_{i_q} + L_f \frac{di_{g_q}}{dt} - \omega_g L_f i_{g_d} \\ U_{dc} \cdot C \frac{dU_{dc}}{dt} = I_C U_{dc} + \frac{3}{2} V_{g_d} i_{g_d} \end{cases} \quad (19)$$

## MACHINE SIDE CONTROL

### Pitch angle control

A discrete conventional proportional-integral (PI) controller [22], depicted in Figure 5, is designed to limit the output power and the relative turbine speed for high wind speed. It adjusts the pitch angle in response to variations in power output according to the following equation.

$$\beta_{ref} = \frac{\Delta\beta}{\Delta P}(P_g - P_{g,rated}) + \beta_0 \quad (20)$$

where: $\beta_0$ is the initial pitch angle.

A first-order transfer function is used within the blade orientation system to ensure the blade position follows the reference signal.

$$\beta = \frac{1}{1+\tau_b s}\beta_{ref} \quad (21)$$

The implemented control strategy is structured as follows:

$$\begin{cases} \beta_{ref} = \beta_0 = 0^\circ \; for \; 0 < P_g \le P_{g,rated} \\ \beta_{ref} = \frac{\Delta\beta}{\Delta\omega}(P_g - P_{g_{rated}}) + \beta_0 \; for P_g > P_{g,rated} \end{cases} \quad (22)$$

### PMSG control

The control of the PMSG is assured via two currents regulators. Under the MPPT control strategy, *isq* is regulated to match the optimal torque reference, while $i_{sd}$ is set to zero to decouple the flux and torque components. The equations governing the generator-side controller are given by:

$$\begin{cases} Ls\frac{di_{sd}}{dt} = K_{p1}(i_{sd}{}^* - i_{sd}) + K_{I1}\varphi_{sd} \\ Ls\frac{di_{sd}}{dt} = K_{p2}(i_{sq}{}^* - i_{sq}) + K_{I2}\varphi_{sq} \\ i_{sd}^* = 0 \\ i_{sq}^* = \frac{T_{em}{}^*}{p\varphi} \\ T_{em}^* = \frac{\frac{1}{2}\rho\pi R^2 V_w^3 C_{pmax}}{\lambda_{opt}} \end{cases} \quad (23)$$

### Gride side control

The grid-side control is carried out by the inverter and is based on controlling the power exchanged with the grid as well as regulating the DC bus voltage. Furthermore, it enables the generation of grid-frequency currents. The control strategy is based on eliminating $i_{gq}$, the q-axis current component. The equations governing the current and voltage control are presented in Equation 24 and Figure 6 illustrates the grid-side control strategy.

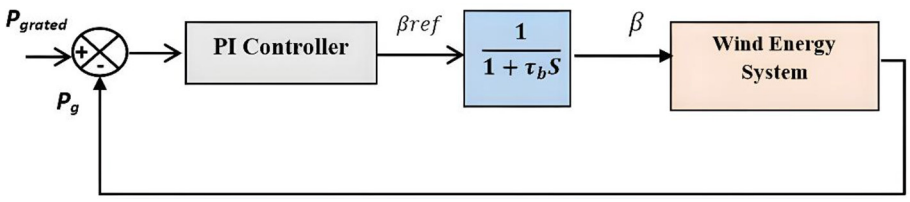


**Figure 5.** Conventional PI pitch control scheme

$$\begin{cases} {i_{gd}}^* = K_{p1}(U^*_{dc} - U_{dc}) + K_{I1}\int(U^*_{dc} - U_{dc})dt \\ i^*_{gq} = 0 \\ {v^*}_{id} = K_{p2}\left(i^*_{gd} - i_{gd}\right) + K_{I2}\int\left(i^*_{gd} - i_{gd}\right)dt - \omega L_f i_{gq} + v_{gd} \\ {v^*}_{iq} = K_{p2}\left(i^*_{gq} - i_{gq}\right) + K_{I2}\int\left(i^*_{gq} - i_{gq}\right)dt - \omega L_f i_{gd} + v_{gq} \end{cases} \tag{24}$$

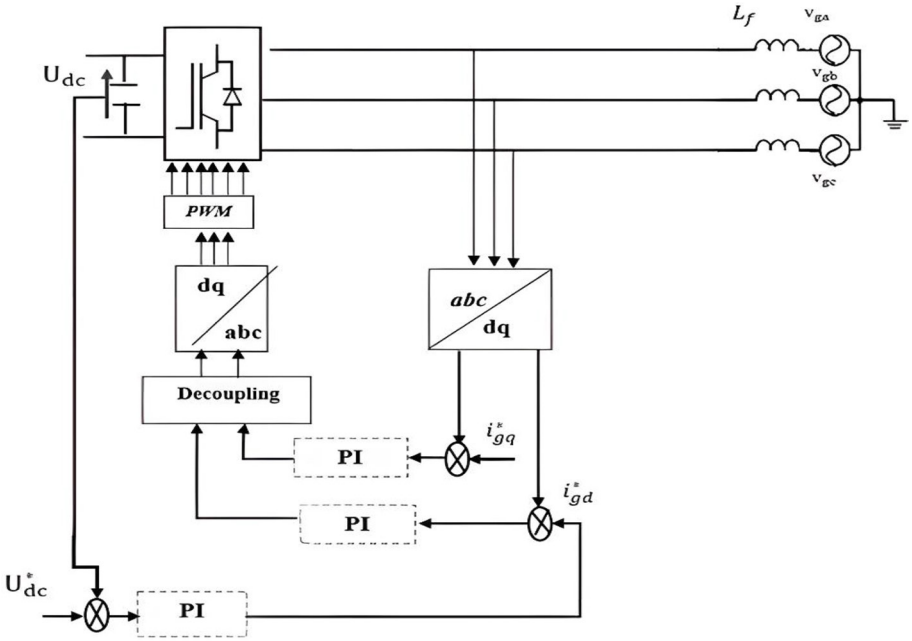


**Figure 6.** Grid side controllers' configuration

## IMPLEMENTATION OF MPPT METHODS FOR WIND TURBINE CONTROL

The objective of the MPPT strategy is illustrated by the static characteristics shown in Figure 7, which represent the developed power relative to the wind turbine rotational speed, as well as the maximum power characteristic representing the connection of the maximum power point for each static characteristic. The aim of the control system is to follow the maximum power curve between the minimum and maximum rotational speeds. Starting from the $V_{cut\text{-}in}$ and by following the maximum power $P_{m\text{-}opt}$ characteristic, the turbine operates at the rotational speed corresponding to the optimal specific speed $\lambda_{opt}$, at which the power coefficient is maximal. The turbine speed is adjusted to harvest maximum wind power. This

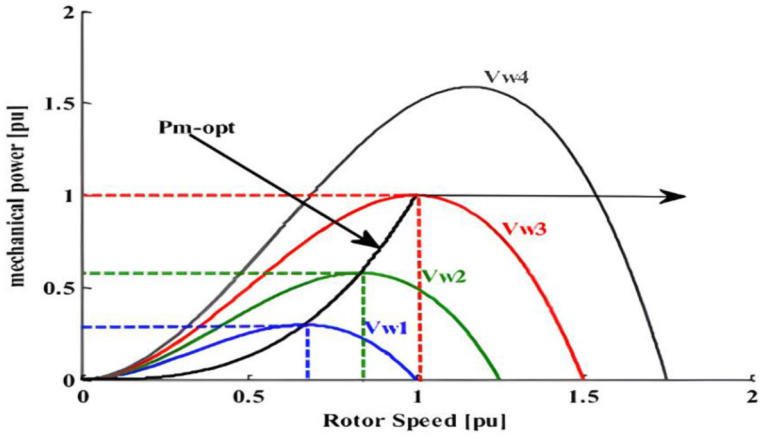


**Figure 7.** Aerodynamic power characteristic [23]

energy is tracked at the maximum power coefficient $C_{(p\_max)}$ using MPPT methods.

## Efficient torque regulation strategies

The proposed approach purposes to enhance the efficiency of the produced power across varying wind speeds. As revealed in Figure 8, the principle of the described technique is regulating the torque corresponding to the optimum torque reference for a specified wind velocity, following the maximum power characteristic curve. In fact, for each wind velocity, the power point tracking method executes a reference torque that allows for the extraction of the MPPT. The studied MPPT technique is shown in the equation:

$$P_{MPPT} = K_{opt}\omega^3 \tag{25}$$

with

$$K_{opt} = \frac{1}{2}\frac{\rho\pi R^5 C_{pmax}}{\lambda_{opt}^3} \tag{26}$$

## CSA technique

This novel technique is inspired by the smart behaviour of crows. In fact, Crows are recognized as highly intelligent birds, capable of recognizing faces and alerting one another when a threatening individual approaches. They demonstrate advanced communication skills and possess long-term memory, enabling them to remember where they have hidden their food. Additionally, crows often follow other crows or birds to locate and steal their hidden food. On the other hand, if a crow realizes it is being followed, it will cleverly change its concealed food location to mislead others and protect its [25, 26]. This paper presents a novel population-based metaheuristic algorithm, termed CSA, inspired by the intelligent behaviors of crows as described earlier. The core principles of CSA are summarized as follows:

- crows live in groups and retain memory of their food hiding locations,
- crows track others to steal their hidden food,
- to protect it, crows move in random patterns.

### *Step 1: define the problem*

For the optimisation problem, decision variables and adjustable parameters are defined are initialized as follows: $N$ – flock size; itermax – the total number of iterations; $AP$ – awareness probability, which determines the likelihood of a crow being aware of being followed and fl – flight length, controlling the distance a crow moves during the search process. The parameters of the CSA given in Table 1 were carefully selected based on a trade-off between convergence speed and solution diversity.

### *Step 2: initialize parameters*

At a given iteration k with N randomly distributed crows, each candidate is represented by a memory $m_i^k$ and a position $x_i^k$ as given in Equations 27 and 28:

$$x_i = [x_1 \ldots\ldots\ldots\ldots x_N] \tag{27}$$

$$m_i = [m_1 \ldots\ldots\ldots\ldots m_N] \tag{28}$$

Assuming that crows have hidden their food in their starting positions, each candidate's memory is initialised.

**Table 1.** Tuning parameters of CSA technique

| Parameters | Values |
|---|---|
| *N* | 4 |
| *AP* | 20.1 |
| *fl* | 1.2 |

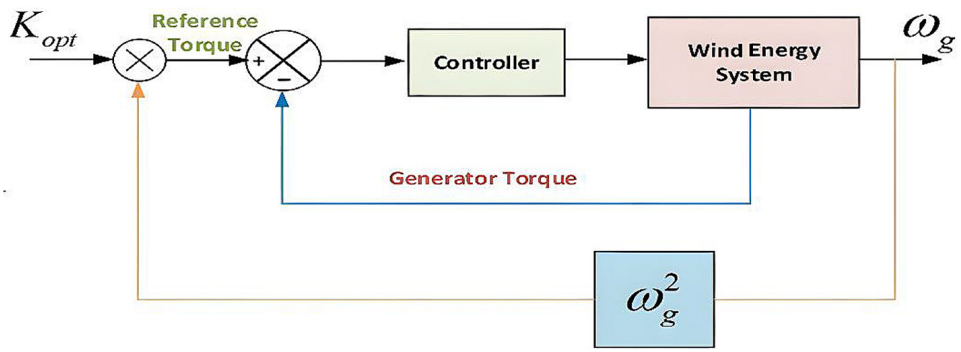


**Figure 8.** MPPT control using the optimal torque control method [24]

*Step 3: evaluate the initial population*

The quality of the initial positions is determined using the fitness function.

*Step 4: create of new candidate's position*

Crow *i* tracks crow j during iteration *k* to locate crow j's hidden food. The positions of the crows are updated based on the AP value, as follows:

- Case1: if $r \geq$ AP, with r is a random number between 0 and 1: this scenario implies that crow j is unaware of being followed by crow *i*. Consequently, the position of crow *i* at iteration (*k*+1) is updated using the following equation:

$$x_i^{k+1} = x_i^k + rfl(m_j^k - x_i^k) \quad (29)$$

- Case 2: $r <$ AP: this scenario implies that crow j becomes aware that crow *i* is tracking it. To deceive crow *i*, crow j adopts a strategy of random movement within the search space. This behavior is mathematically represented by the following equation: $x_i^{k+1}$ = a: random location

Figure 9 provides a representation of the update states and illustrates how the flight length (fl) influences the search capability of the crows.

*Step 5: evaluate the fitness function for newly generated positions*

After updating the position of each crow, the objective function is evaluated for each new position.

*Step 6: update the memory*

The memory of each crow is updated based on the newly evaluated positions as follows.

$$m_i^{k+1} = \begin{cases} x_i^{k+1} \; if fitness(x_i^{k+1}) > fitness(x_i^k) \\ m_i^k \; otherwise \end{cases} \quad (30)$$

The initial values of the position and memory vectors, given by Equations 31 and 32, are applied sequentially:

$$T_{em_i}{}^0 = [Tem_1^0 \, Tem_2^0 \, Tem_3^0 \, Tem_4^0] \quad (31)$$

$$m_i^0 = [m_1^0 \, m_2^0 \, m_3^0 \, \grave{e} m_4^0] \quad (32)$$

The following fitness function expression is used to evaluate the quality of the initial positions:

$$P_g^k = T_{emi}^k . \omega \quad (33)$$

The following expressions are used to update the memory and the positions of each of the four crows.

$$T_{emi}^{(k+1)} = \begin{cases} T_{emi}^k + r \cdot fl \cdot (m_j^k - V_{pvi}^k) \; if \; r \geq AP \\ a \; if r < AP \end{cases} \quad (34)$$

The CSA must be reinitialized to locate the new maxima when sudden variation in the operating point occurs due to change in wind velocities. The proposed method for reinitializing the MPPT technique is based on monitoring changes in electromagnetic torque and output power, as described by Equations 35 and 36, respectively.

$$\left|T_{emi}^{k+1} - T_{emi}^k\right| < \Delta T_{em} \quad (35)$$

$$\left|\frac{P_g^{k+1} - P_g^k}{P_g^k}\right| > \Delta P \quad (36)$$

Figure 10 illustrates the various implementation processes of the implemented MPPT optimization problems.

## SIMULATION MODEL

The simulation results presented in this section provide a detailed assessment of the efficiency of two distinct MPPT control strategies for a 3.6 kW wind turbine system (parameters in Table 2), implemented and analyzed using MATLAB/Simulink. The first method employs a conventional MPPT approach, while the second uses an intelligent optimization technique based on CSA, known for its performance in addressing complex optimization problems. Through detailed simulations, the dynamic response, tracking accuracy,

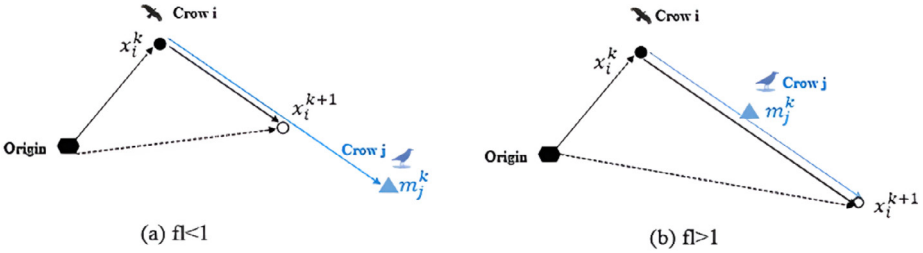


**Figure 9.** Adaptive movement of the crows [27]

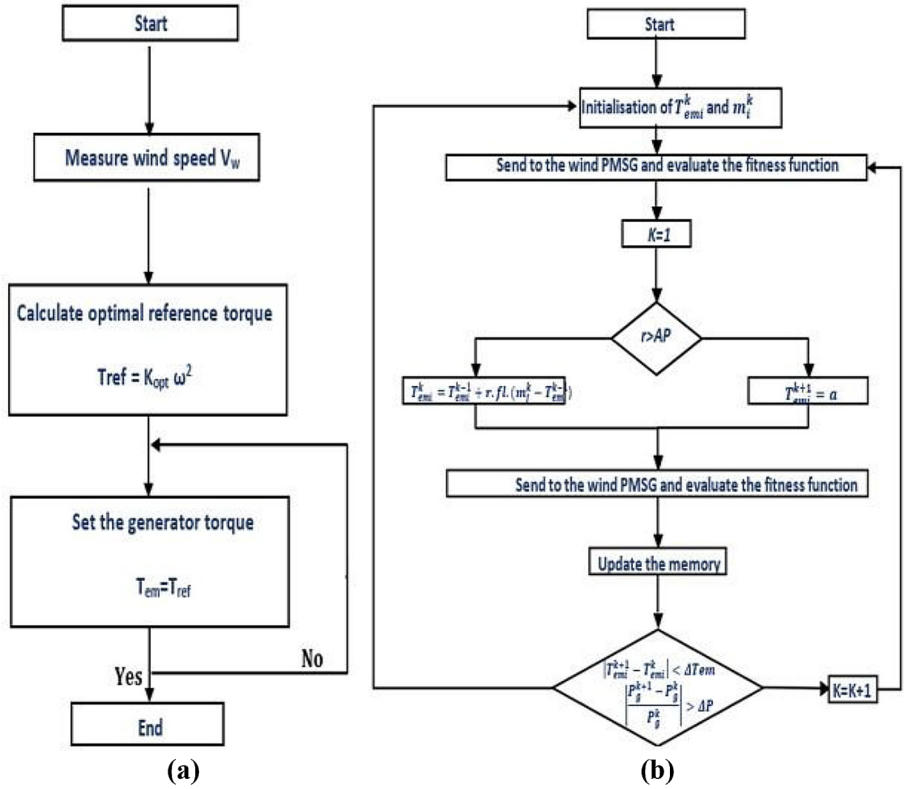


**Figure 10.** Flowchart of the proposed MPPT techniques; (a) Torque regulation technique (b) CSA technique

**Table 2.** Parameters of the studied system

| Parameters | Values |
|---|---|
| $p$ | 1.237 |
| $R$ | 2 m |
| $P$ | 2 |
| $\lambda_{opt}$ | 8 |
| $C_{pmax}$ | 0.473 |
| $R_s$ | 0.82 Ω |
| $L_s$ | 15.1 mH |
| $F$ | $10^{-3}$ N m s $rad^{-1}$ |
| $J$ | 99 $10^{-4}$ kg $m^2$ |
| $\Phi$ | 0.5Wb |
| $P_{nom}$ | 3.6 kW |
| $V_{w0}$ | 10 m/s |
| $\Omega_0$ | 157 rad/s |
| $Tem_0$ | 23 N·m |

and reliability of both methods are compared under varying wind speed conditions.

## Simulation results

During the simulation period of 40 seconds, a variable wind profile ranging from 4 to 13 m/s, averaging10 m/s was applied to the wind turbine model (Figure 11). Beyond this wind speed range, a speed limitation is achieved through the pitch angle regulation, as shown in Figure 12.

The response of the studied structure following the investigated MPPT techniques is provided by the following simulation figures. The response of the electromagnetic torque, given by Figure 13, illustrates the performance of the implemented CSA technique. Indeed, beyond $V_{rated}$ (10 m/s), the torque is adjusted to its nominal value (23 Nm). During this period, it can be deduced that the response of the conventional MPPT method, the torque regulation method, exhibits more fluctuations and a slower response time compared to the intelligent method based on CSA technique.

The response of the angular velocity and the generated power is provided by the following Figure 14 and 15. Both implemented techniques ensure the extraction of the maximum power of 3.6 kW, corresponding to a nominal rotation speed of 157 rad/s, during periods of high wind. The response of the CSA ensures a smoother and faster power extraction.

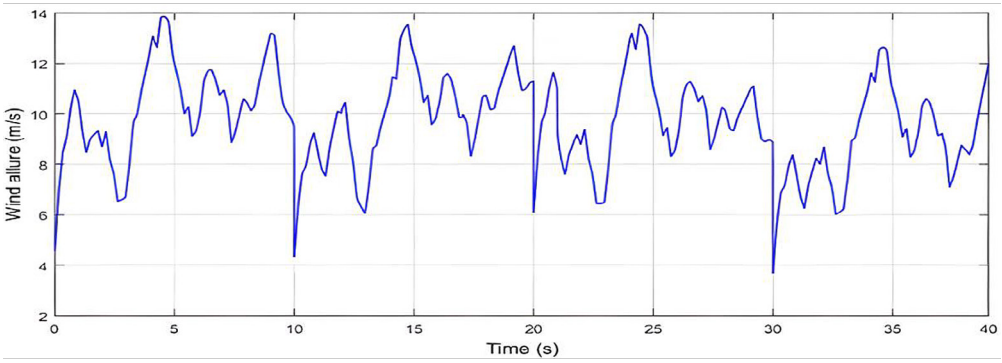


**Figure 11.** Wind speed profile

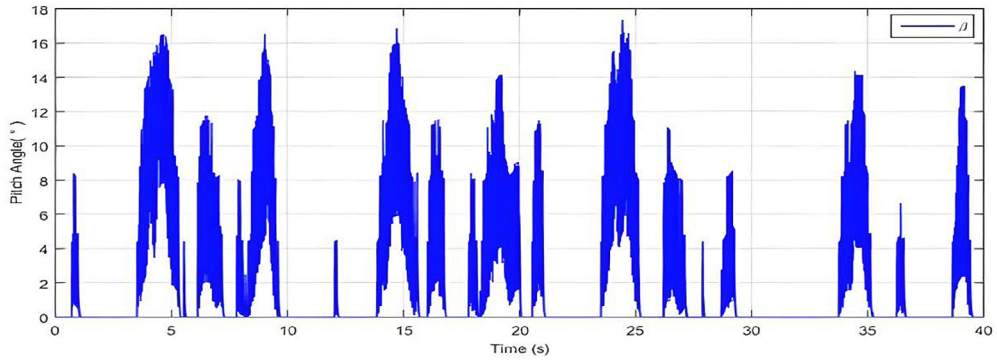


**Figure 12.** Pitch angle response

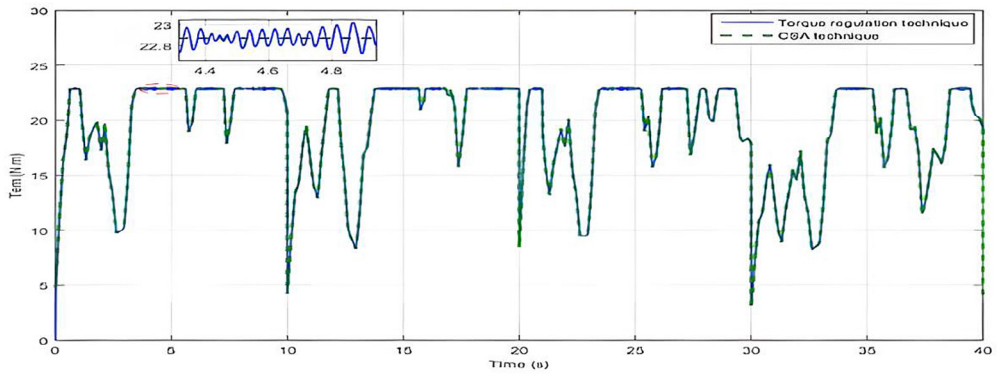


**Figure 13.** Electromagnetic torque response

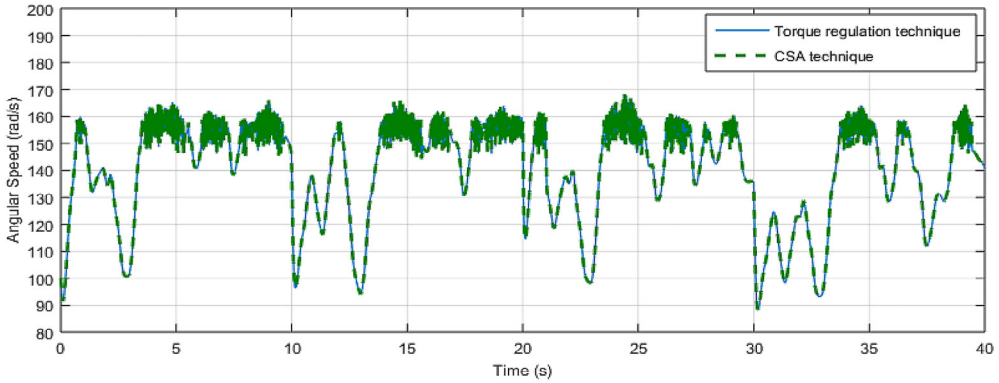


**Figure 14.** Angular speed response

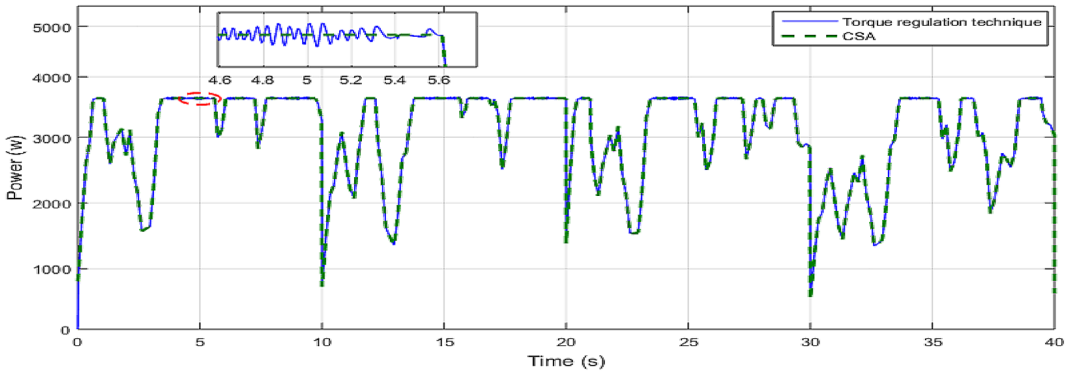


**Figure 15.** Generated power response

To highlight the effectiveness of the grid-side control, simulation figures regarding the DC bus voltage and the grid-side currents and voltages are provided. Indeed, it can be observed in Figure 16 that the DC bus voltage perfectly tracks smoothly its reference value of 400 V, and that the grid quantities depicted in Figure 17 and Figure 18, whether current or voltage, are perfectly three-phase. These responses underscore the robustness of the implemented regulators for the grid-side control.

## Power smoothing analysis

Mitigating output power fluctuations is increasingly important as wind energy systems are increasingly integrated into the grid. As highlighted in [28], The concepts smoothing function are introduced

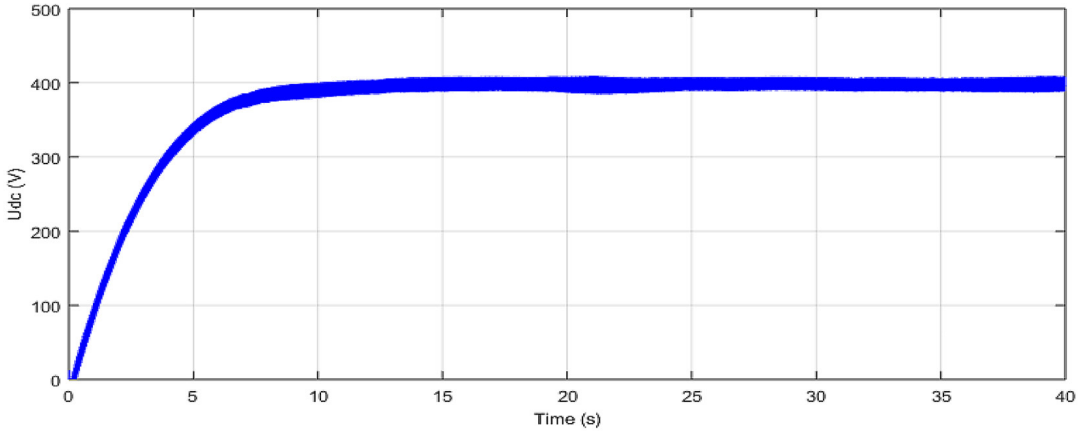


**Figure 16.** DC bus voltage response

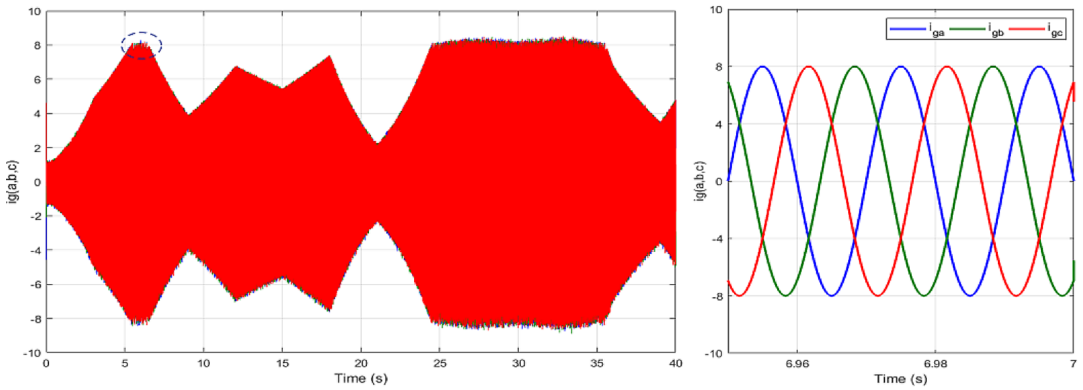


**Figure 17.** Grid currents response

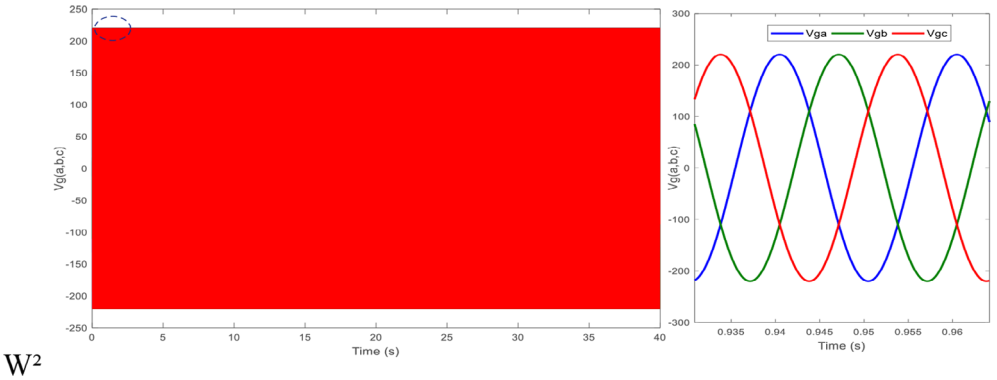


W²

**Figure 18.** Grid voltages response

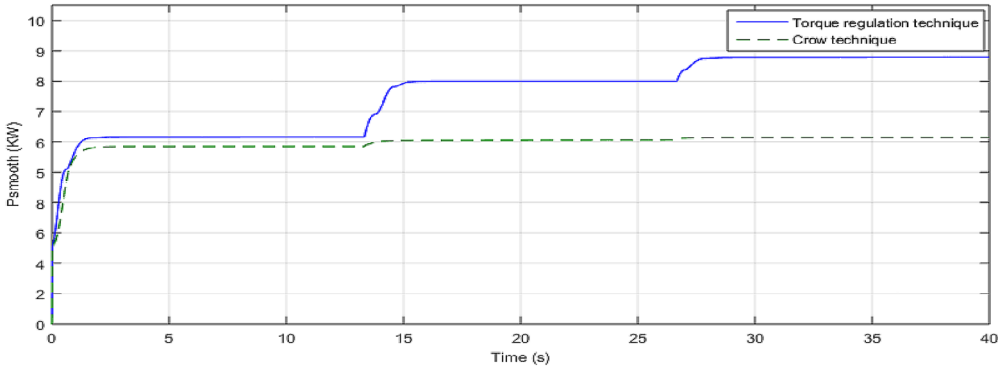


**Figure 19.** $P_{smooth}$ response

and defined using Equation 37 to assess the performance of the suggested based CSA method in smoothing output power given in Figure 19.

$$P_{smooth} = \int_0^t \left| \frac{dP_g(t)}{dt} \right| dt \tag{37}$$

where: $P_{smooth}$ – smoothing power function.

## DISCUSSION

To quantitatively assess the effectiveness of the CSA-based controller, its performance is compared with that of the torque regulation technique. The evaluation is based on key performance metrics, namely the mean squared error (MSE), mean absolute error (MAE), and mean percentage error (MPE). A detailed comparison of the results is presented in Table 3. The CSA-based controller significantly outperforms the conventional method across all indicators. The MPE is reduced by 75%, and the MSE by over 87%, confirming superior accuracy and dynamic response. These improvements result from the adaptive and intelligent search capabilities of the Crow Search Algorithm, which better handles the nonlinearities of the wind energy conversion system. Compared to results reported in previous studies employing PSO or fuzzy-based MPPT controllers [29,30], the CSA-based technique demonstrates similar or improved levels of accuracy, while requiring fewer iterations and showing smoother torque profiles. This confirms the suitability of CSA for real-time MPPT under dynamic wind conditions.

**Table 3.** Comparative performance analysis of MPPT controllers

| Method | MPE(%) | MAE(%) | MSE(%) |
|---|---|---|---|
| CSA | 0.002 | 08.75 | 0.047 |
| Torque regulation technique | 0.008 | 12.02 | 0.38 |

## CONCLUSIONS

In this study, an innovative CSA based MPPT method for grid connected wind turbine systems was proposed and evaluated. This technique has outstandingly performed in convergence speed,

accuracy, and efficiency when tracking the maximum power point under varying wind conditions. Compared to a conventional torque regulation MPPT technique, the proposed method not only improved the generated power output but also ensured smoother and more stable power delivery. Simulation results confirmed that the CSA-based approach effectively reduced power fluctuations, enhancing the overall reliability and quality of the energy harvested from the wind turbine system. These improvements highlight the potential of bio-inspired optimization algorithms, like CSA, in advancing renewable energy technologies. Overall, this study contributes to the advancement of intelligent control strategies that optimize energy extraction and enhance the efficiency of wind energy conversion systems, supporting the transition to more efficient and sustainable energy solutions.

Future work will focus on validating the proposed CSA-based MPPT method using real-time experiments on a physical wind turbine setup. Although the present study is based on detailed simulations to demonstrate the feasibility and performance of the proposed approach, experimental implementation remains a key step toward practical deployment and is planned as part of our ongoing research.

## REFERENCES


1. Da Silva, M.M. Power and Gas Asset Management Regulation, Planning and Operation of Digital Energy Systems. Springer Nature Switzerland AG 2020.
2. Alremali, F.A.M., Yaylacı, E.K., Uluer, İ. Optimization of proportional-integral controllers of grid-connected wind energy conversion system using grey wolf optimizer based on artificial neural network for power quality improvement. Advances in Science and Technology. Research Journal, 2022; *16*(3).
3. Teklehaimanot, Y.K., Akingbade, F.K., Ubochi, B.C., Ale, T.O. A review and comparative analysis of maximum power point tracking control algorithms for wind energy conversion systems. *International Journal of Dynamics and Control*, 2024; 1–23.
4. Kumar, D., Chatterjee, K. A review of conventional and advanced MPPT algorithms for wind energy systems. *Renewable and sustainable energy reviews*, 2016; *55*: 957–970.
5. Pande, J., Nasikkar, P., Kotecha, K., Varadarajan, V. A review of maximum power point tracking algorithms for wind energy conversion systems. *Journal of Marine Science and Engineering*, 2021; *9*(11): 1187.
6. Hannachi, M., Elbeji, O., Benhamed, M., Sbita, L. Comparative study of four MPPT for a wind power system. *Wind engineering*, 2021; *45*(6): 1613–1622.
7. Nouriani, A., Moradi, H. Variable speed wind turbine power control: A comparison between multiple MPPT based methods. *International Journal of Dynamics and Control*, 2022; *10*(2): 654–667.
8. Tiwari, R., Babu, N.R. Fuzzy logic based MPPT for permanent magnet synchronous generator in wind energy conversion system. *IFAC-PapersOnLine*, 2016; *49*(1), 462–467.
9. Yessef, M., Bossoufi, B., Taoussi, M., Lagrioui, A., Chojaa, H. Overview of control strategies for wind turbines: ANNC, FLC, SMC, BSC, and PI controllers. *Wind Engineering*, 2022; *46*(6), 1820–1837.
10. Govinda Chowdary, V., Udhay Sankar, V., Mathew, D., Hussaian Basha, C.H., Rani, C. (2020). Hybrid fuzzy logic-based MPPT for wind energy conversion system. In Soft Computing for Problem Solving: SocProS 2018, Springer Singapore, 2020; 2: 951–968.
11. Minai, A.F., Malik, H. Metaheuristics paradigms for renewable energy systems: advances in optimization algorithms. *Metaheuristic and Evolutionary Computation: Algorithms and Applications*, 2021; 35–61.
12. Bouchakour, A., Zarour, L., Bessous, N., Bechouat, M., Borni, A., Zaghba, L., Ghoneim, S.S. MPPT algorithm based on metaheuristic techniques (PSO & GA) dedicated to improve wind energy water pumping system performance. *Scientific Reports*, 2024; *14*(1), 17891
13. Azzouz, S., Messalti, S., Harrag, A. Innovative PID-GA MPPT controller for extraction of maximum power from variable wind turbine. *Przegląd Elektrotechniczny*, 2019; *95*.
14. Ben Smida, M., Azar, A.T., Sakly, A., Hameed, I.A. Analyzing grid connected shaded photovoltaic systems with steady state stability and crow search MPPT control. *Frontiers in Energy Research*, 2024; *12*: 1381376.
15. Güven, A.F., Samy, M.M. Performance analysis of autonomous green energy system based on multi and hybrid metaheuristic optimization approaches. *Energy Conversion and Management*, 2022; *269*: 116058.
16. Güven, A.F., Yörükeren, N.U.R.A.N., Tag-Eldin, E., Samy, M.M. Multi-objective optimization of an islanded green energy system utilizing sophisticated hybrid metaheuristic approach. *IEEE Access*, 2023; *11*: 103044–103068.
17. Kassa, Y., Zhang, J.H., Zheng, D.H., & Wei, D. A GA-BP hybrid algorithm-based ANN model for wind power prediction. In *2016 IEEE Smart Energy Grid Engineering (SEGE)*, IEEE. 2016; 158–163.
18. Bouaouda, A., Sayouti, Y. Hybrid meta-heuristic algorithms for optimal sizing of hybrid renewable energy system: a review of the state-of-the-art. *Archives of Computational Methods in Engineering*,

2022; *29*(6), 4049–4083.

19. Ganji, E., Mahdavian, M., Eshaghpour, I., Janghorban, M. Designing and modeling of control strategies based on multi-objective optimization for a PMSG wind turbine: a study based on the grid errors and wind speed. Advances in Science and Technology. Research Journal, 2019; *13*(4).
20. Smida, M.B., Sakly, A. Different conventional strategies of pitch angle control for variable speed wind turbines. In 2014 15th international conference on sciences and techniques of automatic control and computer engineering (STA) (pp. 803–808). IEEE, 2014.
21. Smida, M.B., Sakly, A. Fuzzy logic control of a hybrid renewable energy system: A comparative study. Wind Engineering, 2021; *45*(4): 793–806.
22. Ben Smida, M., Sakly, A. Pitch angle control for grid-connected variable-speed wind turbine system using fuzzy logic: A comparative study. Wind Engineering, 2016; *40*(6): 528–539.
23. Ben Smida, M., Sakly, A. Smoothing wind power fluctuations by particle swarm optimization-based pitch angle controller. Transactions of the Institute of Measurement and Control, 2019; *41*(3): 647–656.
24. Goyal, S., Deolia, V.K., Agrawal, S. An advanced neuro-fuzzy tuned PID controller for pitch control of horizontal axis wind turbines. ECTI Transactions on Electrical Engineering, Electronics, and Communications, 2022; *20*(2): 296–305.
25. Abd Elkader, F., Elhady, B., Kalas, A. (2014). Sensor and Sensorless Speed Control of Doubly Fed Induction Generator Wind Turbines for Maximum Power Point Tracking. Port-Said Engineering Research Journal, 2014; *18*(2): 8–16.
26. Meraihi, Y., Gabis, A.B., Ramdane-Cherif, A., Acheli, D. A comprehensive survey of Crow Search Algorithm and its applications. Artificial Intelligence Review, 2021; *54*(4): 2669–2716.
27. Smida, B.M., Azar, A.T., Sakly, A., Hameed I.A. Analyzing grid connected shaded photovoltaic systems with steady state stability and crow search MPPT control. Front. Energy Res., Sec. Solar Energy, 2024; *12*. https://doi.org/10.3389/fenrg.2024.1381376
28. Houam, Y., Terki, A., Bouarroudj, N. An efficient metaheuristic technique to control the maximum power point of a partially shaded photovoltaic system using crow search algorithm (CSA). Journal of Electrical Engineering & Technology, 2021; *16*: 381–402.
29. Borni, A., Bechouat, M., Bessous, N., Bouchakour, A., Laid, Z., Zaghba, L. Comparative study of P&O and fuzzy MPPT controllers and their optimization using PSO and GA to improve wind energy system. International Journal for Engineering Modelling, 2021; *34*(2): 55–76.
30. Chaicharoenaudomrung, K., Areerak, K., Areerak, K., Bozhko, S., Hill, C.I. Maximum power point tracking for stand-alone wind energy conversion system using FLC-P&O method. IEEJ Transactions on Electrical and Electronic Engineering, 2020; *15*(12): 1723–1733.